

Two-photon absorption in potassium niobate

A. D. Ludlow, H. M. Nelson, and S. D. Bergeson

Department of Physics and Astronomy, Brigham Young University, Provo, UT 84602

We report measurements of thermal self-locking of a Fabry-Perot cavity containing a potassium niobate (KNbO₃) crystal. We develop a method to determine linear and nonlinear optical absorption coefficients in intracavity crystals by detailed analysis of the transmission lineshapes. These lineshapes are typical of optical bistability in thermally loaded cavities. For our crystal, we determine the one-photon absorption coefficient at 846 nm to be $\alpha = (0.0034 \pm 0.0022) \text{ m}^{-1}$ and the two-photon absorption coefficient at 846 nm to be $\beta = (3.2 \pm 0.5) \times 10^{-11} \text{ m}^2/\text{W}$ and the one-photon absorption coefficient at 423 nm to be $(13 \pm 2) \text{ m}^{-1}$. We also address the issue of blue-light-induced-infrared-absorption (BLIIRA), and determine a coefficient for this excited state absorption process. Our method is particularly well suited to bulk absorption measurements where absorption is small compared to scattering. We also report new measurements of the temperature dependence of the index of refraction at 846 nm, and compare to values in the literature.

I. INTRODUCTION

For cw laser second harmonic generation in a build-up cavity, thermal issues in the nonlinear crystal inevitably come into play. This is particularly true at high laser powers. In typical applications, a Fabry-Perot build-up cavity increases the fundamental laser intensity by one or two orders of magnitude compared to the single-pass intensity. The nonlinear crystal absorbs a fraction of the fundamental power, heats up, and changes the cavity properties. Thermal lensing changes the cavity's spatial mode. Nonlinear absorption changes the cavity's finesse. Thermal expansion and changes in the crystal's index of refraction change the cavity's optical path length.

These effects are well known, and have been observed by several groups working in this field (for example, [1, 2]). Thermally-induced changes in the build-up cavity sometimes limit the second-harmonic generation efficiency. In many cases, they are nuisances that can be worked around. However, these changes can be used as a sensitive diagnostic tool for accurately characterizing nonlinear crystal properties.

For gases and atomic vapors, measuring optical properties of materials inside Fabry-Perot cavities has a long history [3], particularly in relation to optical bistability, saturable absorption, and index of refraction measurements. Thermal and collisional properties of gases have also been measured in this way [4], as well as optical properties of cavity mirrors [5]. However, measurements of optical properties of crystals in Fabry-Perot cavities is relatively new [6].

In some ways, Fabry-Perot measurements are similar to laser calorimetry [7]. In those calorimetry measurements, a laser passes through a thermally isolated absorbing crystal and heats it slightly. From the temperature rise, laser power, thermal mass, and thermal conductivity it is possible to determine an optical absorption coefficient for the crystal. Comparing calorimetry to our Fabry-Perot measurements, both are photothermal methods. Both can have high sensitivities to small absorptions. In contrast to calorimetry, our “ther-

mometer” is the power-induced shift in the cavity resonance frequency. Fabry-Perot measurements can typically reach much higher intensities, making nonlinear effects more apparent. Furthermore, frequency-based techniques, such as the one presented in this paper, usually offer a higher level of precision.

This paper presents a detailed study of the thermal response of KNbO₃ inside a Fabry-Perot build-up cavity. We use this response to determine a new value for the optical absorption coefficients in KNbO₃ at 846 nm and 423 nm, and to measure the effects of blue-light-induced infrared absorption (BLIIRA). We also measure the temperature-dependence of the index of refraction for light polarized along the *b* and *c* crystal axes. These measurements are compared to values from the literature.

II. EXPERIMENTAL SETUP

Our experimental setup is typical for cw second-harmonic generation in an external build-up cavity (see Figure 1). This laser system is designed for a calcium laser cooling experiment at 423 nm. It produces typically 75 mW at 423 nm, measured outside the cavity.

The laser system consists of a single frequency extended cavity diode laser at 846 nm amplified in a single-pass through a tapered laser diode [8]. The extended cavity diode laser is frequency-stabilized relative to a separate optical cavity using the Pound-Drever method [9] to provide both short and long-term stability. After optical isolation, polarization correction, and mode matching, we inject 200 mW into the Gaussian mode of a four-mirror folded (bowtie) Fabry-Perot frequency doubling cavity. Higher-order modes in the cavity are less than 5% of the Gaussian mode. The input coupler reflectivity is 96.6%, and the other three mirror reflectivities are $> 99.5\%$ in the infrared. The radius of curvature for the two curved mirrors is 100 mm, and they are separated by a distance of 117 mm. The angle of incidence on the curved mirrors is 6.5° , minimizing the ellipticity of the beam waist inside the crystal (41.1 and $40.7 \mu\text{m}$ in the tangential and sagittal planes, as determined from the cavity geometry). The

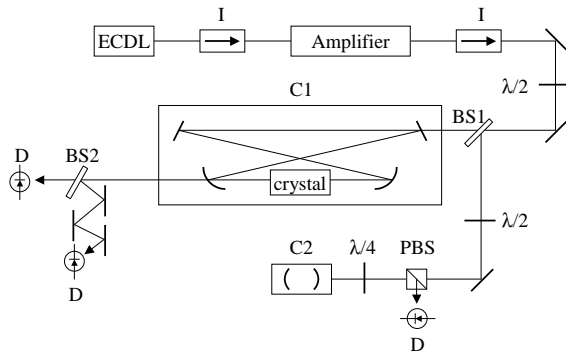


FIG. 1: Schematic diagram of the experimental layout. ECDL = extended cavity diode laser, I = optical isolator, $\lambda/2$ = half wave plate, $\lambda/4$ = quarter wave plate, C1 = frequency doubling “bowtie” cavity, C2 = stable optical cavity, D = photodiode detectors, PBS = polarizing beam-splitter cube, BS1 = uncoated quartz window, BS2 = dichroic beam splitter. The short heavy lines are mirrors.

round-trip cavity length is 618 mm. The KNbO_3 crystal [10] is a -cut and antireflection-coated ($R < 0.25\%$) at 846 nm. The non-critical phase-matching temperature is -11.5°C , for light polarized along the b -axis. The crystal is mounted on a Peltier-cooled copper block. An AD590 temperature sensor and a thermister embedded in the copper mount monitor the crystal temperature. The entire bowtie cavity is enclosed in a sealed aluminum box, filled with dry oxygen at atmospheric pressure. For low laser powers, and when the crystal temperature is far from the phase matching temperature, the cavity finesse with the crystal in place is 124. Without the crystal, the cavity finesse is 140.

III. TRANSMISSION LINESHAPE WITHOUT BLUE LIGHT

When laser light incident on the bowtie cavity is polarized along the c -axis, it is impossible to meet the phase-matching condition for non-critical second harmonic generation at $\lambda = 846$ nm, and no blue light is generated. Previous measurements in KNbO_3 have shown that even small amounts of blue light dramatically change the infrared absorption properties [11, 12, 13]. We address this blue-light-induced-infrared-absorption (BLIIRA) later in the paper. However, in this section we discuss infrared absorption in the *absence* of blue light, *i.e.*: when the incident laser beam is polarized along the c -axis.

One of the flat mirrors in the bowtie cavity is mounted on a piezoelectric crystal, and we use this crystal to change the optical length of the cavity. A small amount of infrared light is transmitted through the cavity mirrors, and we measure this light while sweeping the

cavity length. When the piezo-mounted mirror passes through the position for cavity resonance (*i.e.*: when the roundtrip pathlength in the cavity is an integer multiple of the laser wavelength), the power circulating in the cavity, and transmitted through the cavity end mirror, increases. The transmission lineshape is Lorentzian in the absence of disturbing effects:

$$P(\nu) = \frac{P_0}{1 + F(\nu - \nu_0)^2}, \quad (1)$$

where ν_0 is the resonant frequency of the cavity, $2/\sqrt{F}$ is the full width at half-maximum (FWHM), and P_0 is the infra-red power at the peak of the Lorentzian.

The KNbO_3 crystal inside the bowtie cavity absorbs a small amount of the laser power and heats up. This changes the crystal’s length and index of refraction, which in turn changes the optical path length of the bowtie cavity. We model the overall effect by replacing ν_0 with $\nu_0 + \eta P/P_0$. Accordingly, Equation 1 becomes

$$y = \frac{1}{1 + F(\nu - \eta y)^2}. \quad (2)$$

where $y = P/P_0$ is the normalized transmission, and the frequency ν is measured relative to the unshifted frequency ν_0 . Transmission lineshapes of this kind are typical of optically bistable devices. A similar treatment of this effect is given in the references [6].

The peak in the transmission curve occurs when $y = 1$ and $\nu = \eta$. Figure 2 shows the transmission lineshape for both low and high laser powers. On the same figure we plot a fit of the data to Equation 2. The asymmetry in the transmission lineshape at high powers is due to thermal changes in the optical pathlength. When sweeping the cavity from low to high frequencies as in Figure 2, the power-dependent cavity resonance is effectively “dragged along” from $\nu = \nu_0$ to $\nu = n\nu_0 + \eta$ as the cavity length changes. This is known as “thermal self-locking” [4]. The value of η is called the “self-locking range,” and it is related to the “thermo-optic constant” of reference [6].

For a given power incident on the cavity, we determine the self-locking range η using a nonlinear least-squares fit of the measured transmission lineshape to Equation 2. For the highest laser intensities, it appears that a better overall fit is obtained by replacing ηy in Equation 2 by a higher order polynomial. However, the fit in these high intensity data is hampered because the fit function is not single-valued, as can be seen in Figure 2. For these measurements, we determine the values of η visually by finding the frequency at the peak of the transmission curves.

Our values for η as a function of infrared power in the bowtie cavity are shown in Figure 3a. The error bars indicate the 1σ statistical spread in 5 measurements at each power setting. For linear absorption, the cavity shift, η , should be a linear function of the circulating

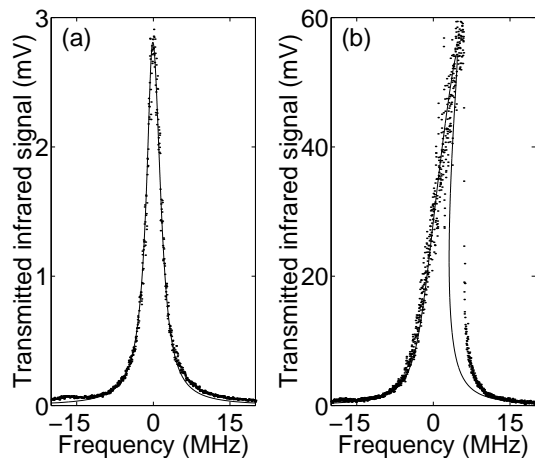


FIG. 2: Infrared transmission lineshape for the bowtie cavity in the absence of blue light. The points are the measurements. The solid line is a fit to the data (see Equation 2). The infrared light is polarized along the c -axis. (a) Low power. (b) High power. For high powers, the fit function is not single-valued above the cavity resonant frequency.

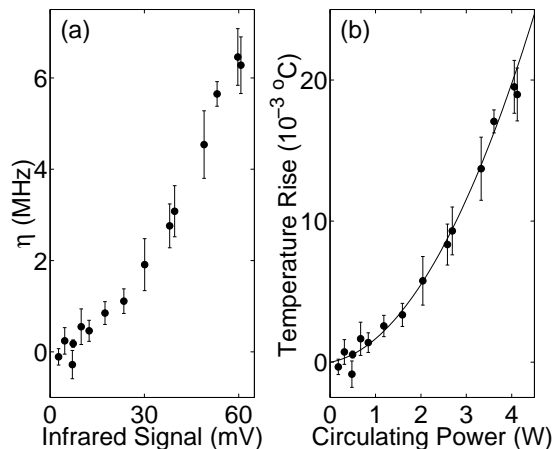


FIG. 3: (a) Self-locking range, η , versus infrared detector signal. (b) The data from 3a with temperature and power calibrations. The solid line is a weighted fit to the data, $T = c_1 P + c_2 P^2$.

power. However our measurements indicate a quadratic dependence of the cavity shift on the circulating power, suggesting that the dominant absorption mechanism is two-photon absorption in the infrared.

We convert η into a temperature rise inside the crystal by measuring the temperature change necessary to shift the cavity resonance frequency by one free spectral range. In these calibration measurements, we attenuate the incident laser power to $10 \mu\text{W}$ to avoid laser-heating in the crystal. The cavity mirror positions remain fixed, and the laser frequency is constant. Using the Peltier device, we change the temperature of the crystal by several degrees while monitoring the cavity transmission. At $T = -11.5^\circ\text{C}$, the resonant frequency of the bowtie cav-

ity shifts at a rate of $231 \text{ MHz } ^\circ\text{C}^{-1}$ for light polarized along the b -axis and $331 \text{ MHz } ^\circ\text{C}^{-1}$ for light polarized along the c -axis.

We calibrate our photodiode signal using a power meter, and measure the efficiency of the optical path to convert this IR signal to a power circulating inside the cavity. The conversion from cavity shift to temperature rise can also be derived from measurements of the change in the index of refraction with temperature. From the published values of dn/dT [14] and the geometry of our bowtie cavity, we calculated what the temperature-dependent shift ought to be. The calculation agrees with our data for the b -axis. However, we find a small difference between the calculation and our data for the c -axis, as discussed later in this paper.

Using our measurements, we convert η into ΔT , the difference in temperature between the crystal axis where the laser propagates and the crystal wall which is kept constant by our temperature control circuit. Figure 3b shows a plot of the temperature rise as a function of the infrared power circulating inside the cavity. It is relatively simple to convert this temperature rise into a measure of the optical absorption coefficient of KNbO_3 by solving the heat transfer equation, which we do below.

IV. SOLVING THE HEAT TRANSFER EQUATION

We solve the heat transfer equation in cylindrical coordinates. The laser beam is in the TEM_{00} Gaussian mode, with a $41 \mu\text{m}$ waist. The confocal parameter of the beam is 6.2 mm , and at the face of the crystal, the beam waist is only 7% larger than in the center of the crystal. So we approximate the laser beam as axially symmetric and Gaussian with a $41 \mu\text{m}$ waist along the entire 10 mm length of the crystal. Our crystal has a square cross section, 3 mm on a side. However, because it is so much larger than the laser beam waist, we assume that the crystal is cylindrical also, with a 1.5 mm radius. With these assumptions, the equilibrium temperature inside the crystal is determined by solving the heat equation in the form:

$$\frac{1}{r} \frac{d}{dr} \left(r \frac{du}{dr} \right) = -\frac{G}{K}, \quad (3)$$

where $u(r)$ is the temperature as a function of radius, G is the power density, and K is the thermal conductivity. Following Sutherland [15], the absorbed power density inside the crystal can be written as

$$G = \alpha I + \beta I^2 \quad (4)$$

where $I = (2P/\pi a^2) \exp(-2r^2/a^2)$ is the laser intensity, P is the laser power incident on the crystal, a is the Gaussian beam waist, α is the linear optical absorption

coefficient, and β is the two-photon absorption (TPA) coefficient.

We can simplify Equation 3 by letting $r = ay/\sqrt{2}$, $A = (P\alpha/2\pi K)$, and $B = (P^2\beta/2\pi^2a^2K)$. With these substitutions, Equation 3 integrates once to

$$\frac{du}{dy} = \frac{A}{y} [\exp(-y^2) - 1] + \frac{B}{y} [\exp(-2y^2) - 1], \quad (5)$$

where the constant of integration is chosen to avoid a singularity as $y \rightarrow 0$. The solution to this differential equation is

$$u(y) = -\frac{A}{2} E_1(y^2) - \frac{A}{2} \ln(y^2) - \frac{B}{2} E_1(2y^2) - \frac{B}{2} \ln(y^2) + C \quad (6)$$

where $E_n(x)$ is the exponential integral [16], and C is the constant of integration. This constant is determined by requiring the temperature at the wall of the crystal to be T_c (*i.e.*: $u(r = b) = T_c$), which we control in the experiment. With this constraint, we can evaluate the temperature rise on axis inside the crystal. The series expansion for the exponential integral has a logarithmic term that exactly cancels the $\ln(y^2)$ terms in Equation 6.

$$\begin{aligned} \Delta T &= u(0) - T_c = \frac{A}{2} \left[\ln\left(\frac{2b^2}{a^2}\right) + \gamma \right] + \frac{B}{2} \left[\ln\left(\frac{2b^2}{a^2}\right) + \gamma + \ln(2) \right] \\ &= \frac{\alpha}{4\pi K} \left[\ln\left(\frac{2b^2}{a^2}\right) + \gamma \right] P + \frac{\beta}{4\pi^2 a^2 K} \left[\ln\left(\frac{4b^2}{a^2}\right) + \gamma \right] P^2, \end{aligned} \quad (7)$$

where $\gamma = .57721 \dots$ is Euler's constant.

We can analyze the data in Figure 3 to extract the linear and two-photon absorption coefficients. A weighted fit to the function $T(P) = c_1P + c_2P^2$, gives $c_1 = (5.7 \pm 3.6) \times 10^{-4} \text{ }^\circ\text{C W}^{-1}$ and $c_2 = (1.09 \pm 0.12) \times 10^{-3} \text{ }^\circ\text{C W}^{-2}$. The uncertainties in these numbers are the statistical uncertainty from the weighted fit to the data. Taking the thermal conductivity from [7] $K = 4.0 \text{ W m}^{-1} \text{ }^\circ\text{C}^{-1}$, $a = 41 \times 10^{-6} \text{ m}$, $b = 1.5 \times 10^{-3} \text{ m}$, and $\gamma = 0.57721$. We determine the one-photon (linear) absorption coefficient to be $\alpha = (0.0034 \pm 0.0021) \text{ m}^{-1}$ and the two-photon absorption coefficient to be $\beta = (3.16 \pm 0.35) \times 10^{-11} \text{ m W}^{-1}$. The uncertainties in these absorption coefficients are only statistical. We have a systematic uncertainty in the power measurements of 10%. Our assumption of cylindrical symmetry in the crystal for solving the heat equation also introduces an error. The error is known, but related to this is the fact that our laser does not propagate exactly down the center of the crystal. These errors show up in the $\ln(b^2)$ term in Equation 7, and probably add $\sim 8\%$ uncertainty to the measurements. Our best numbers for the absorption coefficients are therefore $\alpha = (0.0034 \pm 0.0022) \text{ m}^{-1}$ and $\beta = (3.2 \pm 0.5) \times 10^{-11} \text{ m/W}$. These numbers do not reflect the uncertainty in the thermal conductivity, which we do not know. To our knowledge, this is the first determination of the two-photon absorption coefficient at any wavelength in KNbO₃.

Earlier work on the linear absorption coefficient for KNbO₃ [7] found $\alpha = 0.001 \text{ cm}^{-1} = 0.1 \text{ m}^{-1}$ at 860 nm. This value is much higher than this work. It may be that some of the absorption measured in previous work was two-photon absorption. That work used laser calorimetry to measure the absorption coefficient at specific laser lines

from 457 nm to 1064 nm. At 860 nm, they focused a 900 mW laser beam into a 5 mm crystal, and it is likely that the intensity was high enough for multiphoton absorption to be important.

Our method for determining the one and two-photon absorption coefficients is quite general. It is independent of measurements of light scattering inside the crystal. It is also independent of reflection measurements at the crystal faces. This method is particularly well suited to measurements of optical absorption where the absorption coefficients are comparable to or smaller than scattering and reflection coefficients.

V. TRANSMISSION LINESHAPE WITH BLUE LIGHT

When infrared light incident on the bowtie cavity is polarized along the b -axis of the KNbO₃ crystal, it is possible to meet the phase-matching conditions required for generating the second harmonic at 423 nm. The presence of blue light in the crystal dramatically alters the transmission lineshape. Not only is the blue light itself absorbed by the crystal, it also significantly increases the absorption of the infrared light. This is called "blue-light-induced-infrared-absorption" (BLIIRA), and it has been studied at length in the literature [7, 11, 12, 13]. Previous work has found BLIIRA to be significant at blue light intensities down to $7 \times 10^{-4} \text{ W/cm}^2$. BLIIRA is minimized at longer wavelengths and at higher crystal temperatures [13]. However, for our calcium work, we require high powers at 423 nm.

As before, we fix the laser frequency and scan the cavity length through the resonance condition. Both blue

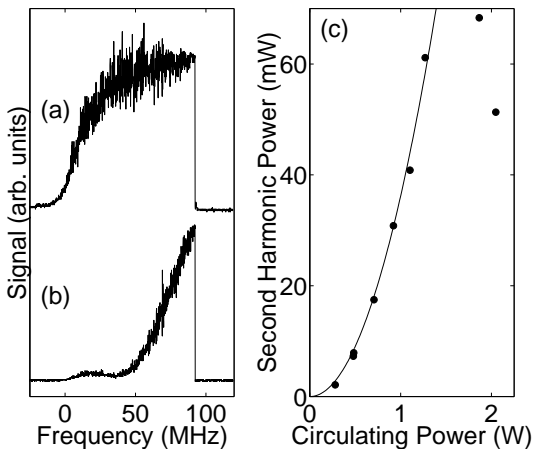


FIG. 4: (a) Cavity transmission lineshape in the infrared at 846 nm when generating the second harmonic at 423 nm. This signal is taken from the highest intensities in the experiment. Note that for low powers, the FWHM is 5 MHz. (b) The second harmonic signal for the same settings as 4a. The shoulder to the left of the signal is a Maker fringe (see text). (c) Peak second harmonic power as a function of peak infrared power. For all but the highest two power measurements, the peak blue power is given by $P_{blue} = 36.2\text{kW}^{-1} P_{ir}^2$.

light at 423 nm and a small amount of infrared light at 846 nm exits the cavity. We separate these wavelengths using dichroic mirrors, which transmit 95% in the blue and reflect 99.5% in the infrared. To make sure that no blue light reaches the infrared laser beam detector, we use four of these mirrors in series in the infrared beam path after the doubling cavity (see Figure 1).

In these experiments, we do not independently control the infrared and blue beam intensities. Rather, we optimize the crystal temperature to maximize the blue light production for each infrared power setting in the steady state. Losses inside the doubling cavity limit the maximum infrared power circulating inside and therefore the maximum blue light produced.

The transmission lineshape for the cavity when blue light is present is shown in Figure 4a for our highest IR powers. The temperature rise inside the crystal is significant. At maximum power, as the cavity approaches the resonance condition, only a small amount of blue light is initially generated because the crystal temperature is too low to meet the phase matching condition for second harmonic generation exactly (see Figure 4b). Closer to the cavity resonance condition, the circulating power increases, the crystal heats up, and more blue light is generated, which heats the crystal even more. This positive feedback continues, and the cavity demonstrates thermal self-locking for up to 90 MHz, as shown in Figure 4a.

The blue light signal in Figure 4b has a shoulder on the low-frequency side of the maximum. This is a Maker fringe. As stated previously, we initially optimize the crystal temperature for optimum blue light production in the steady state. At the highest intensities, the tem-

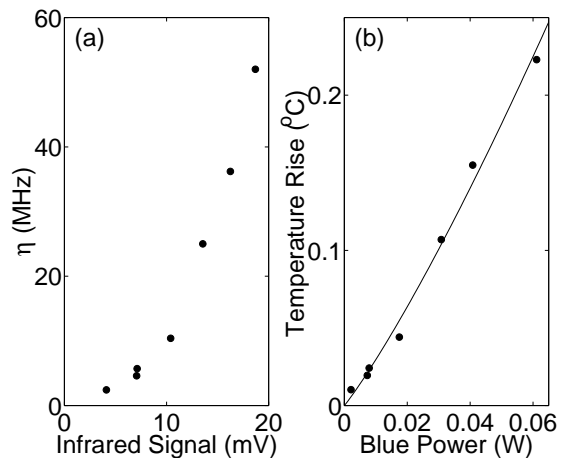


FIG. 5: (a) Self-locking range, η , in the presence of blue light versus infrared detector signal, excluding the highest power data where the SHG process appears to be saturating. (b) The data from 5a with the temperature and power calibrations, and with the temperature rise from the infrared light subtracted off. The solid line is a weighted fit to the data (see text).

perature shift ($\sim 0.4^{\circ}\text{C}$) due to thermal self-locking of the cavity is a few times the temperature phase matching bandwidth.

Because of these complicated thermal conditions, and especially because the blue light production is not constant across the transmission lineshape, we are reluctant to fit the lineshape to any model for the highest laser intensities. Instead, we find the self-locking range graphically. It is the falling step at the far right hand side of the infrared transmission peak shown in Figure 4. This choice is valid as long as there is no significant thermally-induced change in the cavity coupling efficiency. We can monitor these changes by measuring the light reflected from the cavity. For the relatively modest intensities in this study, the minimum reflected light (which corresponds to the maximum light inside the cavity) changes by only a few percent, and only at the highest intensity measurements. The statistical scatter in the data is larger than this, and we neglect this small systematic error.

At lower laser intensities, where BLIIRA and other absorption processes are less severe, we use a least-squares method similar to Section 3 to find the self-locking range η . The self-locking range is plotted as a function of infrared laser power in Figure 5a. Note that except for the two highest power measurements, the frequency doubling process is not saturated (see Figure 4c).

With blue light present in the crystal, the temperature rise inside the crystal has three sources: infrared absorption (one and two photon), blue light absorption, and BLIIRA. We can easily subtract off the infrared contribution to the self-locking range using the data in Figure 3 as a look-up-table. The remaining contribution to the self-locking range is due to temperature rise from blue

light absorption and BLIIRA.

Because the blue light intensity and the temperature are not constant along the length of the axis of the crystal, we must be careful about how we define the temperature rise and the blue light intensity. We will define the absorption coefficient at 423 nm, δ , by the equation

$$\Delta P = \int_V I_b \delta dV = \delta P_b L \quad (8)$$

where I_b is the blue light intensity inside the crystal, P_b is the measured blue power, and L is the length of the crystal. In the non-depleted pump plane-wave approximation, the blue light intensity grows quadratically with distance z in the crystal. With the definition from Equation 8, the blue light intensity can be written as $I_b(r, z) = (12P_b z^2 / \pi a^2 L^2) \exp(-4r^2/a^2)$, where a is the Gaussian waist for the infrared beam in the crystal and we explicitly assume that the Gaussian waist for the blue beam is $a/\sqrt{2}$.

The heat equation for blue light absorption and BLIIRA is written as

$$\frac{1}{r} \frac{\partial}{\partial r} \left(r \frac{\partial u}{\partial r} \right) + \frac{\partial^2 u}{\partial z^2} = -z^2 \left(C e^{-4r^2/a^2} + D e^{-6r^2/a^2} \right). \quad (9)$$

The first term on the right hand side of the equation is the blue light absorption term where $C = 12P_b \delta / (\pi a^2 L^2 K)$. The second term on the right hand side of the equation is the BLIIRA term, where $D = 24P_b P_{ir} \xi / (\pi^2 a^4 L^2 K)$, P_{ir} is the measured infrared power, assumed to be constant along the crystal length, and ξ is the BLIIRA absorption coefficient. As before, $u(r, z)$ is the temperature inside the crystal and K is the thermal conductivity.

The solution of this equation for $r = 0$ is

$$\Delta T(z) = \frac{3\delta}{4\pi K} \left[\ln \left(\frac{4b^2}{a^2} \right) + \gamma \right] \frac{z^2}{L^2} P_b + \frac{\xi}{a^2 \pi^2 K} \left[\ln \left(\frac{6b^2}{a^2} \right) + \gamma \right] \frac{z^2}{L^2} P_b P_{ir}, \quad (10)$$

but we have to be careful about how we define the temperature rise. In Equation 9, the radial derivatives are much larger than the longitudinal derivatives, and the $\partial^2 u / \partial z^2$ term can be treated perturbatively. This approximation produces a temperature function that increases quadratically with z in the crystal.

We can write the temperature rise on axis as $\Delta T(z) = T^m z^2 / L^2$, where T^m is the maximum temperature rise in the crystal. We can calculate the change in the optical pathlength inside the crystal with this temperature profile. It is equal to the change in pathlength due to an equivalent temperature $\Delta T' = T^m / 3$. More expressly, we can write $T(z) = T^m z^2 / L^2 = 3T' z^2 / L^2$, and rewrite Equation 10 as

$$T' = \frac{\delta}{4\pi K} \left[\ln \left(\frac{4b^2}{a^2} \right) + \gamma \right] P_b + \frac{\xi}{3a^2 \pi^2 K} \left[\ln \left(\frac{6b^2}{a^2} \right) + \gamma \right] P_b P_{ir}, \quad (11)$$

Knowing this, we can convert the measured self-locking range of the cavity in the presence of blue light into a temperature rise. The data is plotted in Figure 5. For this data, the ‘‘temperature rise’’ is the average temperature rise in the crystal, i.e.: T' . The ‘‘blue power’’ is the measured blue power, i.e.: the power at the end of the crystal, P_b .

Again, we fit a function of the form

$$\Delta T = a_1 P_b + a_2 P_b P_{ir} \quad (12)$$

to the data in Figure 5b using a multivariable least-squares method and find $a_1 = 2.41^\circ\text{C W}^{-1}$ and $a_2 = 1.04^\circ\text{C W}^{-2}$. Using equation 11, we determine the absorption coefficients $\delta = 13.3 \text{ m}^{-1}$ and $\xi = 2.2 \times 10^{-8} \text{ m/W}$. Apparently, there are no measurements in the literature of the KNbO₃ absorption coefficient at 423 nm. However, there are measurements close to this wavelength [7], and a value of 13.3% per cm is reasonable. For this determination of the absorption coefficient, we have the same kinds of uncertainties as before, namely in the beam position in the crystal and in the power measurement. We estimate the error in this measurement to be 15%. Our final number for the absorption coefficient at 423 nm is $\delta = (13 \pm 2) \text{ m}^{-1}$.

This uncertainty estimate is perhaps conservative. We have a second KNbO₃ crystal. In a simple transmission measurement at 423 nm, using the blue light after the frequency doubling cavity, we find the linear absorption coefficient to be 13% per cm, in agreement with the work above.

We verified the validity of our perturbative approximation by solving Equation 9 numerically. In the numerical solution, the temperature profile is quadratic in z except at the very end of the crystal, where it flattens out slightly to meet the boundary condition of no heat flowing out the crystal face. With our values of δ , ξ , a , P_b , and P_{ir} , the calculated temperature T' agrees with our data to about one percent.

It is interesting that the above treatment of BLIIRA does not distinguish between blue-light induced infrared absorption and infrared light induced blue-light absorption. This model of BLIIRA only postulates that there is a two-color two-photon absorption cross-section. This treatment of two-color two-photon absorption in KNbO₃ is perhaps simplistic. However, it serves the purpose in this paper of demonstrating that thermal self-locking of a Fabry-Perot cavity can be used to sensitively characterize the linear and nonlinear optical properties of an absorbing crystal.

VI. NEW MEASUREMENTS OF dn/dT

From the calibration measurements that convert η in Figures 3 and 5 to a temperature rise, we can extract the temperature-dependent change in the index of refraction for KNbO_3 . When the crystal temperature changes, the optical pathlength of the bowtie cavity also changes because both the crystal length and the index of refraction depend on temperature:

$$\frac{d\mathcal{L}}{dT} = L_c \left[\frac{dn_x}{dT} + \alpha_T (n_x - n_0) \right], \quad (13)$$

where \mathcal{L} is the cavity optical pathlength, L_c is the crystal length (10 mm), α_T is the coefficient of linear expansion for KNbO_3 , and n_x and n_0 are the indices of refraction for the crystal and air, respectively.

In a relatively simple measurement, we can determine dn/dT for the crystal across a wide range of temperatures. We fix the laser frequency and the cavity mirror positions. We attenuate the laser intensity to $10\mu\text{W}$ to avoid thermal self-locking. The crystal temperature can be independently controlled because it is mounted on a Peltier device. We measure the cavity transmission while slowly sweeping the crystal temperature over several degrees. At certain temperatures, the cavity optical pathlength meets the resonance condition, and we measure a peak in the cavity transmission. The temperature between transmission peaks in these measurements corresponds to changing the optical pathlength by one optical wavelength, 846 nm. We repeat these measurements over a wide temperature range to determine $d\mathcal{L}/dT$ from -12°C to about 50°C .

Using equation 13, we convert $d\mathcal{L}/dT$ to dn/dT . With $n_c = 2.13$, $n_b = 2.28$, $\alpha_T = 5 \times 10^{-6} \text{ }^\circ\text{C}^{-1}$, and $d\mathcal{L}/dT = \lambda/\Delta T$, we determine dn/dT for several temperatures. Our values are shown in Figure 6 for light polarized along the c -axis and b -axis, as labeled. Also shown in the figure is the data from Ghosh [14]. The line from Ghosh is a fit to his measurements of the index of refraction between 0 and 140°C . We extrapolate that fit to lower temperatures to compare with our data.

For light polarized along the c -axis, our measurements agree with those of Ghosh over our entire temperature range. For light polarized along the b -axis, in the range 5 to 50°C , which is roughly the range for which our data overlaps Ghosh's data, our measurements also agree. However, below $\sim 5^\circ\text{C}$, our data departs slightly from Ghosh's.

To check our data, we made an additional measurement. When the polarization of the light incident on the cavity is rotated slightly relative to the c -axis, the transmission lineshape has two features, one for each polarization. Because the index of refraction is different for the two polarizations (b and c), the optical pathlength is also different, and each polarization is transmitted at a different cavity length. When we change the temperature

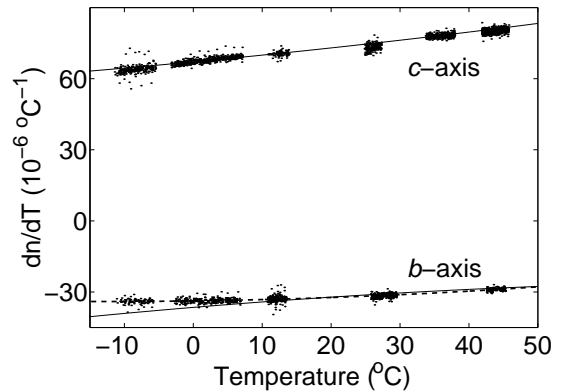


FIG. 6: The change in the index of refraction with temperature for light polarized along the b and c -axes. The points are from this work. The solid line is from Ghosh [14]. The dashed line is a second order polynomial fit to the data.

of the crystal, the two peaks in the transmission lineshape shift by different amounts in different directions, as shown in Figure 7. We measured these shifts for a set of small temperature changes near -11.5°C and determined the relative changes in the indices of refraction, $(dn_c/dT) / (dn_b/dT)$. These measurements confirm our low temperature data in Figure 6. Following the treatment of Ghosh, we fit our dn/dT data for the b -axis to a second-order polynomial, and find

$$\begin{aligned} \frac{dn_b}{dT} = & 1.55809 \times 10^{-9} T^2 \\ & + 4.06912 \times 10^{-8} T - 33.76305 \times 10^{-6} \end{aligned} \quad (14)$$

where the units of dn/dT are $^\circ\text{C}^{-1}$, and T is measured in Celsius.

VII. CONCLUSION

We have demonstrated how thermal self-locking of a Fabry-Perot cavity can be used to determine optical properties of nonlinear crystals. We have determined new values for the one- and two-photon absorption coefficients in KNbO_3 at 846 nm. We have also determined new values for the one photon (linear) absorption coefficient at 423 nm, and a BLIIRA absorption coefficient under specific circumstances. Finally, we present new measurements of the temperature-dependent change in the indices of refraction for the b and c axes.

These measurements all derive from the thermal response of an absorbing Fabry-Perot cavity to light circulating in the cavity. The methods are general and can be widely applied to other systems, particularly those in which the absorption coefficients are small compared to scattering and reflection coefficients.

VIII. ACKNOWLEDGEMENTS

We express our appreciation to Ross Spencer for his computational assistance. This work is supported in part by a grant from the Research Corporation and from the National Science Foundation under Grant No. PHY-9985027.

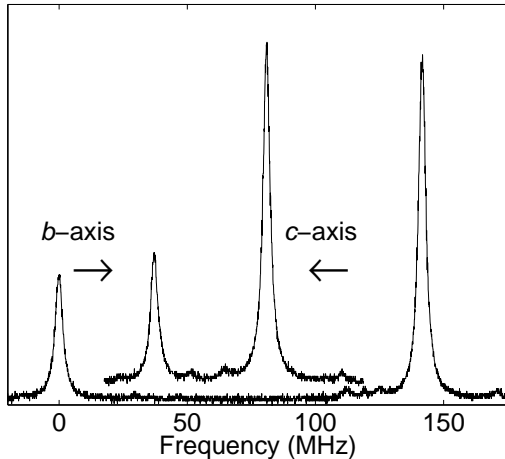


FIG. 7: Transmitted lineshape as a function of cavity length for two temperatures. The upper trace has been displaced for clarity. The polarization of the light incident on the cavity is rotated a few degrees relative to the c -axis. The larger feature is polarized along the c -axis, and the smaller feature is polarized along the b -axis, as labeled. This shows the magnitude and direction of the change in the cavity resonance length with temperature.

-
- [1] A. Arie, S. Schiller, E. K. Gustafson, and R. L. Byer, "Absolute frequency stabilization of diode-laser-pumped Nd:YAG lasers to hyperfine transitions in molecular iodine," *Opt. Lett.* **17**, 1204-1206 (1992)
- [2] E. S. Polzik and H. J. Kimble, "Frequency doubling with KNbO₃ in an external cavity," *Opt. Lett.* **16**, 1400-1402 (1991)
- [3] A. E. Siegman, *Lasers*, (University Science Books, Mill Valley, CA), 1986.
- [4] P. Dube, L.-S. Ma, J. Ye, P. Jungner, and J. L. Hall, "Thermally induced self-locking of an optical cavity by overtone absorption in acetylene gas," *J. Opt. Soc. Am. B* **13**, 2041-2054 (1996).
- [5] K. An, B. A. Sones, C. Fang-Yen, R. R. Dasari, M. S. Feld, "Optical bistability induced by mirror absorption: measurement of absorption coefficients at the sub-ppm level," *Optics Letters*, **22**, 1433-1435 (1997)
- [6] A. Douillet, J.-J. Zondy, A. Yeliseyev, S. Lobanov, and L. Isaenko, "Stability and frequency tuning of thermally loaded continuous-wave AgGaS₂ optical parametric oscillators," *J. Opt. Soc. Am. B* **16**, 1481-1495 (1999)
- [7] L. E. Busse, L. Goldberg, M. R. Surette, and G. Mizell, "Absorption losses in MgO-doped and undoped potassium niobate," *J. Appl. Phys.* **75** 1102 (1994).
- [8] Our extended cavity laser is a Vortex laser from New Focus Corp. (5215 Hellyer Ave., Suite 100 San Jose, CA 95138-1001). The tapered amplifier is a Model 8613 laser from SDL (80 Rose Orchard Way San Jose, CA 95134-1365) with the rear cavity optics removed, configured as a single-pass amplifier.
- [9] R. W. P. Drever, J. L. Hall, F. V. Kowalski, J. Hough, G. M. Ford, A. J. Munley, and H. Ward, "Laser phase and frequency stabilization using an optical resonator," *Appl. Phys. B* **31**, 97-105 (1983).
- [10] Our crystal is from VLOC, 7826 Photonics Drive, New Port Richey, FL 34655, U.S.A.
- [11] L. Goldberg, L. E. Busse, and D. Mehuys, "High power continuous wave blue light generation in KNbO₃ using semiconductor amplifier seeded by a laser diode," *Appl. Phys. Lett.* **63**, 2327-2329 (1993).
- [12] H. Mabuchi, E. S. Polzik, and H. J. Kimble, "Blue-light-induced infrared absorption in KNbO₃," *J. Opt. Soc. Am. B* **11**, 2023-2029 (1994).
- [13] L. Shiv, J. L. Sorensen, and E. S. Polzik, "Inhibited light-induced absorption in KNbO₃," *Opt. Lett.* **20**, 2270-2272 (1995).

- [14] G. Ghosh, "Dispersion of thermo-optic coefficients in a potassium niobate nonlinear crystal," *Appl. Phys. Lett.* **65**, 3311-3313 (1994).
- [15] R. L. Sutherland. *Handbook of Nonlinear Optics* (Dekker, New York, 1996), p. 502
- [16] M. Abramowitz and I. A. Stegun, *Handbook of Mathematical Functions* (Dover, New York, 1970), p. 228